



BEAM INDUCED QUENCH STUDY OF
TEVATRON DIPOLES

R. Dixon, N.V. Mokhov*, and A. VanGinneken
August 1980

Abstract

A series of tests are reported which study the quench behavior of Tevatron dipoles under irradiation. Various types of beam spill and loss modes are investigated for 350 and 400 GeV proton beams and for magnet currents from 500 to 3000 A. Spatial distributions of energy deposition in superconducting magnets are calculated using two independent Monte Carlo programs. Experimental and calculational data are in good agreement and some regularities are observed.

*Institute for High Energy Physics, Serpukhov, USSR



Introduction

One of the main problems confronting the Tevatron is radiation heating in superconducting magnets.¹⁻⁴ This paper reports results of a series of measurements made on a string of two Tevatron dipoles. Various types of beam spill and loss modes are investigated for 350 and 400 GeV proton beams and for magnet currents ranging from 500 to 3000 A. Spatial distributions of energy deposition in the magnets are calculated using two independent Monte Carlo programs.

Experiment

The experiment, performed in the Meson beam line of the Fermilab switchyard, uses two Tevatron dipoles as shown in figure 1. The magnets MH250-1 and MH250-2 are installed in a long drift space and connected in series with opposite polarities so as to form a horizontal dog leg in the beam. Four conventional dipoles, HT250-1-4, also in the beam line form a dog leg that exactly cancels the displacement resulting from the superconducting magnets. This configuration allows the beam line to be operated with any choice of current in the Tevatron magnets from 0 to 4000 A. Figure 2 shows a typical beam trajectory through the magnets.

The magnets are cooled using the switchyard satellite refrigerator which is capable of providing up to 400 watts of refrigeration through 200 feet of liquid helium transfer lines. The power leads to the magnets are also contained in the transfer line. An operating temperature of $4.7^{\circ} \pm .1^{\circ}$ is maintained by keeping the single phase helium passage filled with subcooled liquid.

Two methods of data accumulation are used to make the measurements discussed here. In the first, beam is passed straight through the magnets as shown in figure 2 with the quench resulting from beam losses associated with the beam halo. In the second method a remotely controlled copper target .25" thick is inserted in the beam just upstream of HT250-1. Measurements are made with three spill lengths,

20 μ sec, 1 ms, and .5 sec. Beam profiles are obtained before each datum is recorded by inserting a remotely controllable segmented wire ionization chamber (SWIC) into the beam just upstream of MH250-1. Figure 3 shows the beam profiles for 20 μ sec spill and .5 sec spill. The wire spacing is 1 mm. The SWIC is removed before the datum is recorded to avoid additional beam losses due to the presence of the SWIC.

Additional beam instrumentation includes a set of two foot long, two inch diameter ionization chambers which serves as beam loss monitors (LM), a halo detector which consists of an ionization chamber that surrounds the beam pipe, and the main ring extraction secondary emission monitor and toroid to measure beam intensities. Output data from all of these devices are recorded for every beam pulse by the main ring data logging system on the X-530 computers. "Snap-shot" data are also recorded on a PDP-11 computer. These data give a continuous picture of magnet currents and voltages as well as some of the loss monitors beginning within 10 seconds before the quench and ending within 10 seconds after the quench. These data are useful in determining which of the two magnets quenched.

Before each measurement the beam is tuned through the magnets with $I=0$ in both HT-250 and MH250. The intensity is then reduced to 1×10^{12} protons per pulse and the beam is turned off. At this point the desired current is established in HT-250 and MH250 and the beam is turned back on. The beam intensity is then raised in small steps until a quench is obtained. For each step beam intensity and loss monitor data are recorded. The beam intensity corresponding to the quench is reported as the average value of the intensity in the last two steps with an error equal to the difference between them. Refrigeration data for the point are taken at the beginning of the run before the superconducting magnets are powered. This includes temperatures and pressures in the magnets as well as in the remainder of the cryogenic system.

Calculations

The energy deposition in the superconducting magnets under irradiation is calculated using two independent Monte Carlo programs viz., CASIM⁵ and MARS-6^{4,6}. Both programs simulate the full three dimensional development of hadronic cascades and allow for the presence of magnetic fields. Both programs use inclusive descriptions for hadron production: the thermodynamical model in CASIM and phenomenological formulae in MARS. MARS transports particles from interaction to interaction and treats different materials by exactly locating their interface. CASIM traces particles in small steps and boundary crossings are resolved over distances roughly equal to that of the step size. As a consequence of this last difference the complex geometry is more simply described in CASIM.

In general results of both calculations agree well. However, for the present application one important difference arises. It concerns the description of electromagnetic showers from π^0 -decay. In MARS-6 this is treated using an empirical formula which has no provision for magnetic fields. The present version of CASIM includes program AEGIS⁷ which simulates electromagnetic showers in detail with or without fields. Note that the present version MARS-8⁸ is also capable of simulating electromagnetic showers with the AEGIS program.

A rough simulation of the experiment with the program MARS-6 predicts the maximum energy density in MH250-1 to be about 5×10^{-4} GeV/g (inc. proton). Using empirical enthalpy data¹ this is within a factor of two of the observation and of the CASIM results.

The geometry description encoded in the program CASIM is shown in figure 4. The proper curvature of the Tevatron dipoles is included. The only gross simplification in the geometric description occurs in the cryogenic "turnaround box", just upstream of the superconducting magnets (labeled "TAB" in figure 4). In the program this is represented by a uniformly dense annulus.

The magnetic field in the conventional dipoles is assumed to be constant in the aperture and to vanish elsewhere. For the superconducting dipoles the field is described by a map covering the entire cross section of the magnet. In all cases the beam is assumed to have normally distributed density profiles with vertical and horizontal standard deviations, $\sigma_v = 2.5$ mm and $\sigma_h = 6$ mm, respectively.

A major uncertainty in this study is the extent and spatial distribution of beam halo. In the present experiment the effect of a halo containing a total number of particles outside the aperture equal to a few percent of the beam is comparable to that of particles produced in the target. All calculated results shown below are exclusive of halo. This must be borne in mind in the comparison with data.

Results of the CASIM calculations for various values of incident energy and magnetic fields are shown in Figs 5-9. For clarity only the energy density in the inner region of the coil and for the azimuthal region near the beam plane are plotted as a function of distance along the beam. These contain the highest energy densities encountered in the calculation. The bin size is sufficiently small to reflect variations of the energy density with location.

For 400 GeV incident energy and a magnetic field of 3 Tesla, the radial dependence near the shower maximum is shown in Fig. 10, and the azimuthal variation in the inner radial region is plotted in Fig. 11.

Figure 12 shows the relative importance of the electromagnetic component in the inner radial region and for two azimuthal regions.

Data and Interpretation

Twenty five measurements are reported from two separate study periods. These data are shown in Table I. Eight of the points do not correspond to quenches but instead to lower limits as the intensity could not be raised high enough to obtain a quench. The first study period corres-

ponds to 400 GeV incident beam and $I_q \geq 1500$ A. The second study period uses 350 GeV incident beam for $I_q < 1500$ A.

The loss monitor, LM (4042) is arranged in a standard geometry used throughout the switchyard so that results from it are applicable to predicting beam loss problems at other locations. The output of this loss monitor is expected to be approximately proportional to the incident beam intensity. Figures 13-15 show the output of LM(4042) plotted vs the current at which the magnets quenched, I_q , for the three types of beam spill incident on the copper target. The figures indicate that there is little difference between the 1 ms and the 20 μ s spill data. There is approximately a factor of four difference between slow and 20 μ sec spill.

Figure 16 shows beam intensity vs I_q for the 20 μ sec spill copper target. This looks quite similar to figure 13. Also shown on the plot are predictions based on the maximum energy density obtained in the shower calculations. Agreement of calculation and experiment is better than within a factor of two. Table II lists the results of the calculations for all currents and beam energies.

To determine quench properties from energy deposition it is necessary to know the enthalpy reserve, ΔH , in the superconducting coil. There are two sources: the measurements of Edwards et al¹, and theoretical estimates (see for example Ref. 4).

The values of ΔH for the region around the maximum energy deposition under present conditions are presented in Table II. It can be seen that data from two sources disagree especially at lower currents up to a factor of two. The reason is not clear.

The number of incident protons needed to induce a quench is

$$N_i = \frac{\Delta H}{1.6 \cdot 10^{-7} E_{\max} \eta},$$

where η is the efficiency of the target. In the present case of a 0.25" thick copper target $\eta = 0.04$. The formula is valid only for fast spill < 1 msec. The values of N_i for 20 μ sec spill are presented in Table II.

The determination of tolerable beam losses for longer spill is a more difficult problem. It requires thermo-physical data of the superconducting coil and helium, and solving the three dimensional transient heat transfer problem. In this paper only instantaneous heating is calculated.

The shower calculation is used to obtain the energy density required to quench the magnets. This allows comparison of these results with other experiments^{1,2} analyzed in similar fashion. The enthalpy reserve in the superconducting coil does not enter in this comparison. Such a comparison is presented in figure 17. Edwards et. al.¹ used calorimeter measurements to obtain energy density. The other points rely on CASIM calculations. All of the data exhibit good agreement and all lie above the theoretical estimate. The agreement between different measurements is quite remarkable in view of the different geometries, beams and magnets used in the experiments.

In conclusion it appears that the quench properties of superconducting magnets can be predicted quite reliably for short spill durations. For longer spill times the short spill data provide at least a lower limit on the tolerable energy deposition.

We would like to thank Helen Edwards for her many contributions to the work reported in this paper. We are also very indebted to the entire Fermilab Switchyard Group for their aid in carrying out this experiment.

References

- 1) H. Edwards, et al., IEEE MAG-13, N.1 (1977) p. 666.
- 2) B. Cox, P.O. Mazur, A. VanGinneken, IEEE NS-26, N3 (1979) p. 3885.
- 3) H. Edwards, S. Mori, A. VanGinneken, UPC-30 (1978).
- 4) M.A. Maslov, N.V. Mokhov, Preprint IHEP 79-135, Serpukhov, 1979. To be published in "Particle Accelerators", 1980.
- 5) A. VanGinneken, FNAL Report FN-250 (1972), FN-272 (1975).
- 6) N.V. Mokhov, Proc. of IV All-Union Conference on Charge Particle Accelerators, Moscow, 1974, Vol 2, M. Nauka, 1975, p. 222. I.S. Baishev, S.L. Kuchinin, N.V. Mokhov, Preprint IHEP 78-2, Serpukhov, 1978.
- 7) A. VanGinneken, FNAL Report FN-309 (1978).
- 8) N.V. Mokhov, FNAL Report FN-328 (1980).

TABLE I

Pt	I (amp)	Eo	Spill	Type
1	1500	400	20 μ s	Copper Target
2	1500	"	1 ms	" "
3	1500	"	.5 sec	" "
4	3000	"	1 ms	Straight Through
5	3000	"	20 μ s	" "
6	2000	"	.5 sec	Copper Target
7	2000	"	1 ms	" "
8	2000	"	20 μ s	" "
9	1500	"	"	" "
10	3000	"	"	" "
*11	1500	"	.5 sec	Straight Through
*12	1500	"	1 ms	" "
*13	1500	"	20 μ s	" "
*14	2000	"	.5 sec	" "
*15	2000	"	1 ms	" "
*16	2000	"	20 μ s	" "
*17	3000	"	.5 sec	" "
*18	3475	"	.5 sec	" "
19	500	350	20 μ s	Copper Target
20	500	350	20 μ s	" "
21	750	"	20 μ s	" "
22	1000	"	20 μ s	" "
23	1500	"	20 μ s	Copper Target

*No quench obtained for these points.

TABLE II

QUENCH INDUCED LOSSES
400 GeV PROTONS INCIDENT ON TARGET

+20%

	MH250	$\Delta H,^*$	ϵ_{\max}'	Ni, **
	Current,	mJ/g	GeV/g	ppp
	Amps			$\tau = 20 \mu \text{ sec}$
$E_0 = 350 \text{ GeV}$	500	(4)	.0015 \pm .0003	4.7×10^{11}
	750	¹¹ (3.6)	.0013 \pm .0003	1.32×10^{12} (4.33×10^{11})
	1000	7 (3.2)	.0012 \pm .0002	9.1×10^{11} (4.17×10^{11})
$E_0 = 400 \text{ GeV}$	1500	5. (2.5)	.0010 \pm .0002	7.8×10^{11} (3.9×10^{11})
	2000	2.7 (1.8)	.0010 \pm .0002	4.22×10^{11} (2.8×10^{11})
	3000	1.3 (0.9)	.0011 \pm .0002	1.85×10^{11} (1.28×10^{11})

*Based on H. Edwards et. al.¹ Values in brackets are theoretical estimates.

**Number of incident protons needed to produce quench for target efficiency $\eta = 0.04$ (0.63 cm Cu target).

FIGURE CAPTIONS

- Fig. 1 Experimental layout of the superconducting magnets, MH250-1 and MH250-2, as well as the conventional trim magnets, HT250-1-4. Beam instrumentation including loss monitors, the SWIC, and the halo detector is also shown.
- Fig. 2 Horizontal magnet apertures are shown with a typical beam trajectory.
- Fig. 3 Typical beam profiles observed in the SWIC for 20 μ sec spill and .5 sec spill. The horizontal profiles are on the left.
- Fig. 4 Geometry description used in the program CASIM showing from the copper target to the upstream superconducting magnet.
- Fig.5-9 Energy density distributions from the program CASIM for various values of magnetic field and incident beam energy.
- Fig. 10 Radial dependence of the energy deposition near the shower maximum for 400 GeV incident beam and a 3 Tesla magnetic field in the superconducting magnets.
- Fig. 11 The azimuthal dependence of the energy density near the inner radial region.
- Fig. 12 Fraction of energy deposited by electromagnetic showers in the inner radial region for the two azimuthal regions.
- Fig. 13 Quench current vs LM (4042) voltage for all of the quenches induced by 20 μ sec spill on the copper target at both 350 and 400 GeV. The straight line is a least squares fit to the 400 GeV points only.

- Fig. 14 Quench current vs. LM (4042) voltage for quenches induced by 1 ms spill incident on the copper target. The 3000 A point corresponds to a quench of the superconducting leads rather than a magnet quench. The straight line is the least squares fit to the 20 μ sec data.
- Fig. 15 Quench current vs. LM (4042) voltage for all quenches induced by .5 sec spill incident on the copper target. The two highest points are beam halo points rather than copper target points, and do not correspond to quenches. They are therefore lower limits on the allowable loss monitor voltage. The straight line is 3.75 x the least squares fit to the 400 GeV 20 μ sec data.
- Fig. 16 Quench current vs. incident beam intensity for all of the quenches induced by 20 μ sec spill on the copper target. Crosses indicate the predictions of the beam intensity required to induce a quench from the shower calculation.
- Fig. 17 Comparison of the energy density required to quench superconducting magnets from three experiments. The points are plotted vs. I/I_{\max} where I_{\max} is the maximum current possible in the magnet.

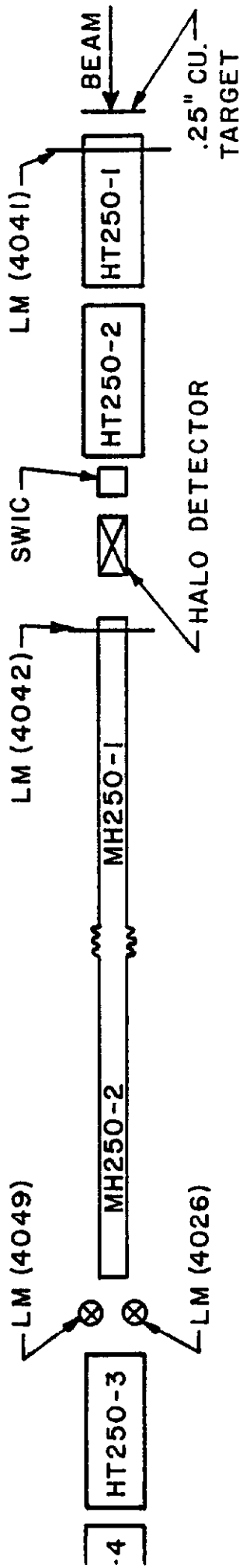


Fig. 1

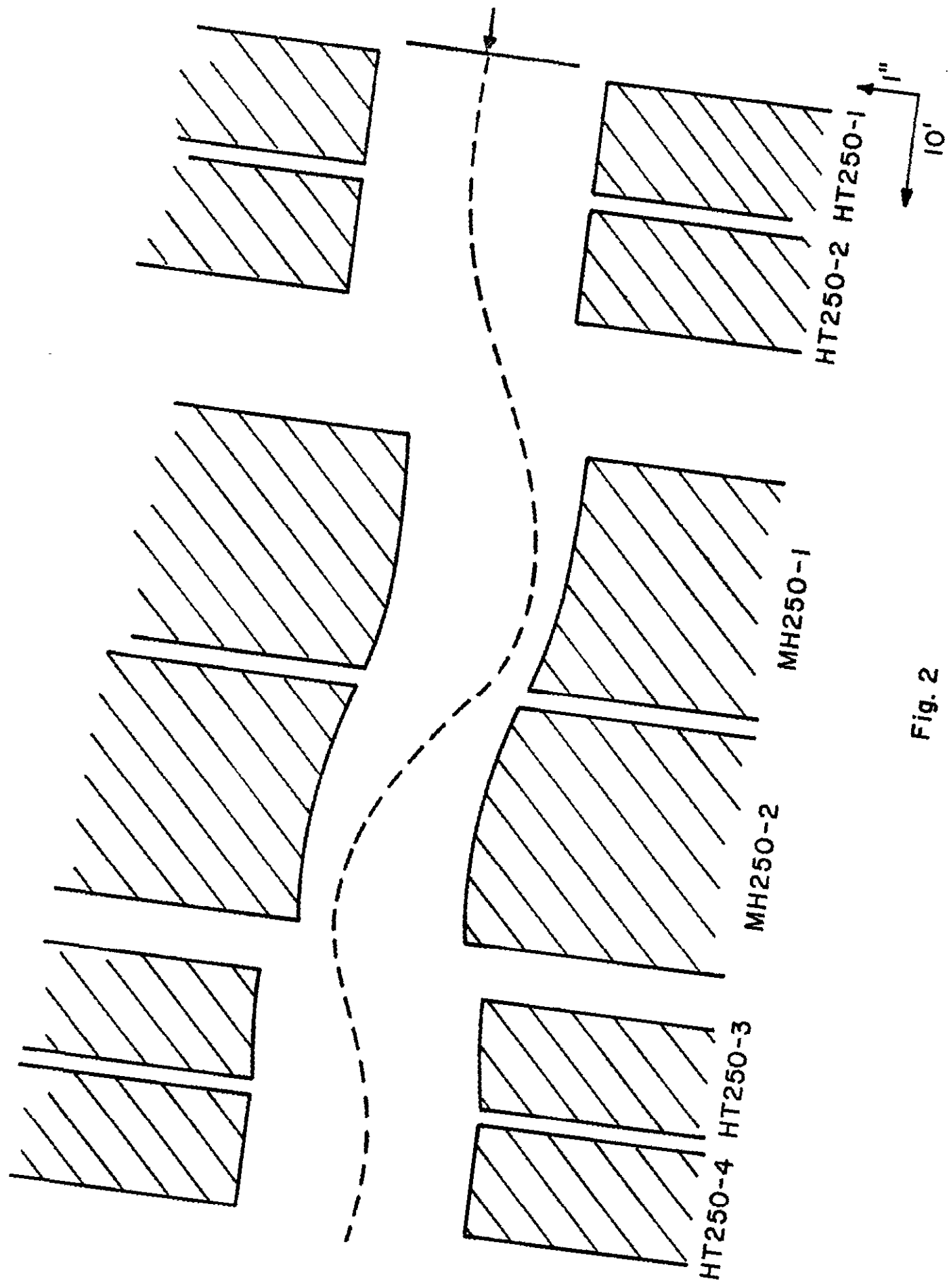
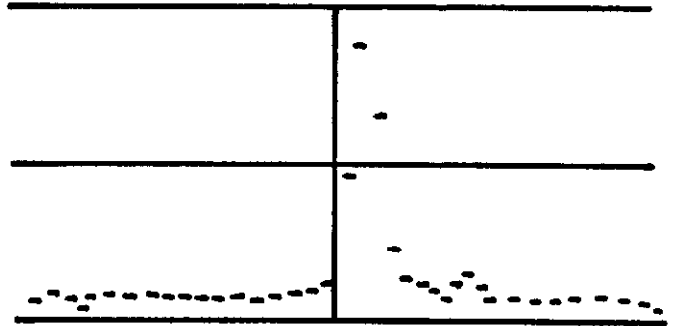


Fig. 2

MQ201 SWIC

20 μ Sec
1500 amps



.5 Sec
1500 amps

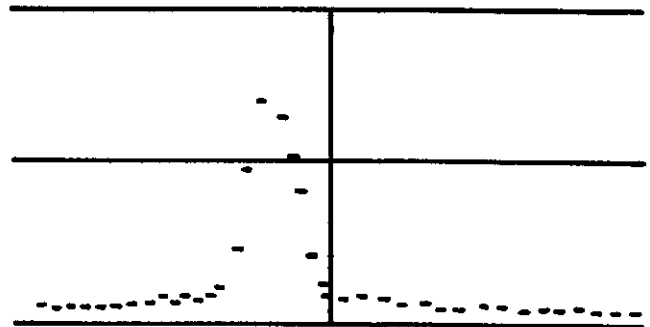


Fig. 3

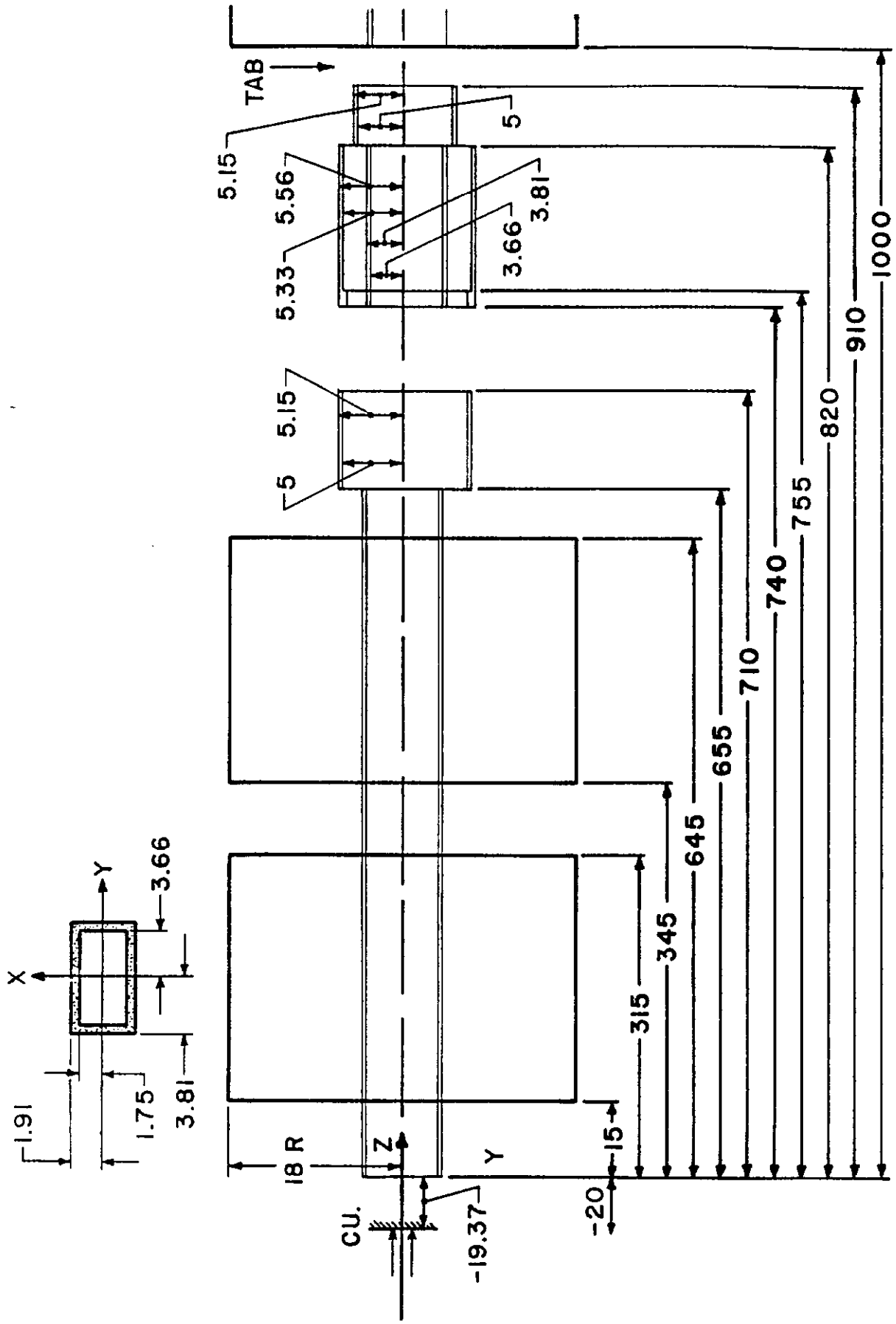


Fig. 4

Beam: $\sigma_v = 2.5$ mm

$\sigma = 6.0$ mm

Target: .63 cm Cu

$Z_0 = -20$ cm

○

○ $0 \leq \phi \leq 0.1$

● $-3.0416 \leq \phi \leq 3.1416$

$3.81 \leq r \leq 4.30$

350 GeV

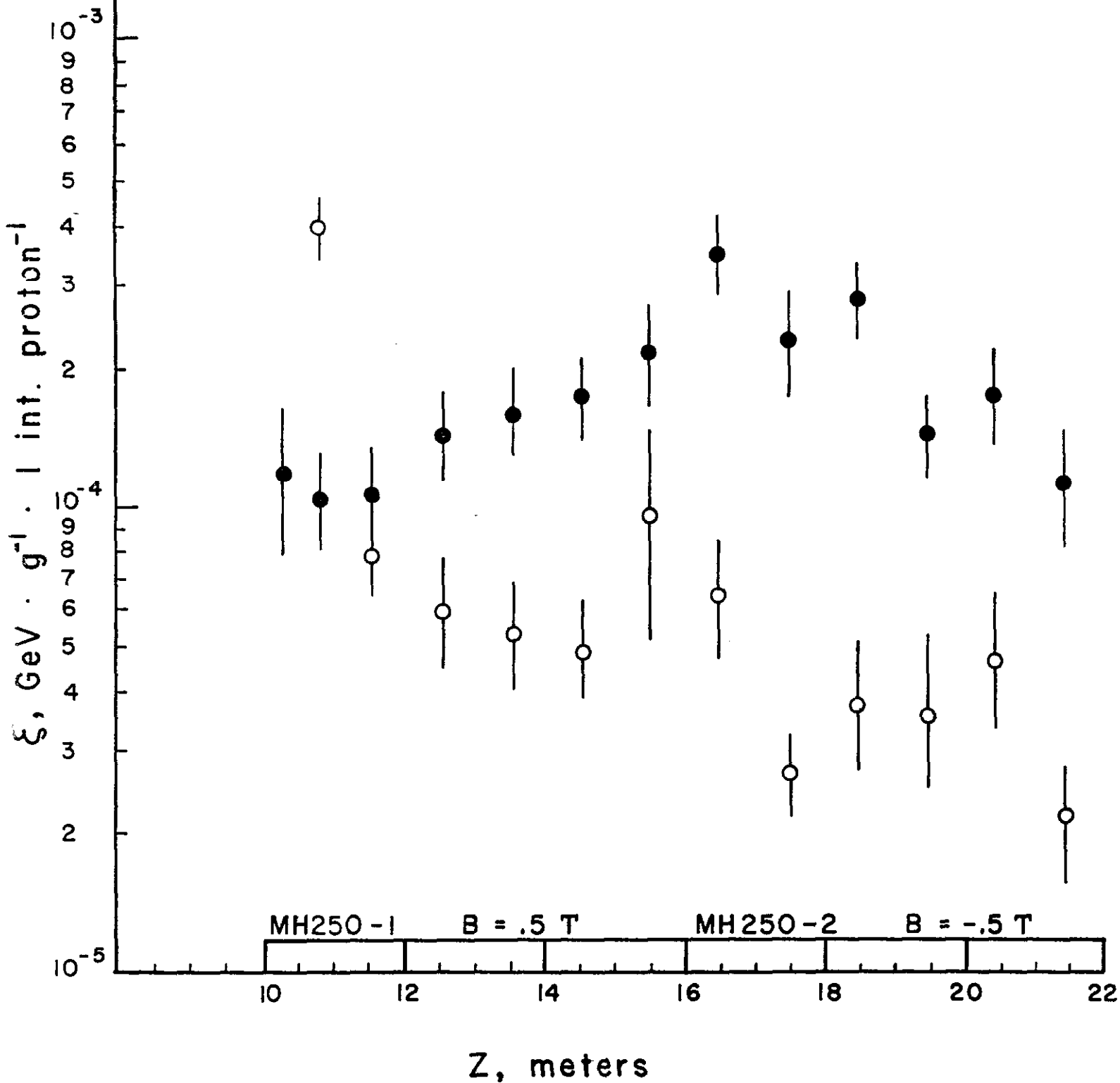


Fig. 5

Beam: $\sigma_V = 2.5$ mm

$\sigma_H = 6.0$ mm

Target: .63 cm Cu

$Z_0 = -20$ cm

○ $0 \leq \phi \leq 0.1$

● $-3.0416 \leq \phi \leq 3.1416$

$3.81 \leq r \leq 4.30$

350 GeV

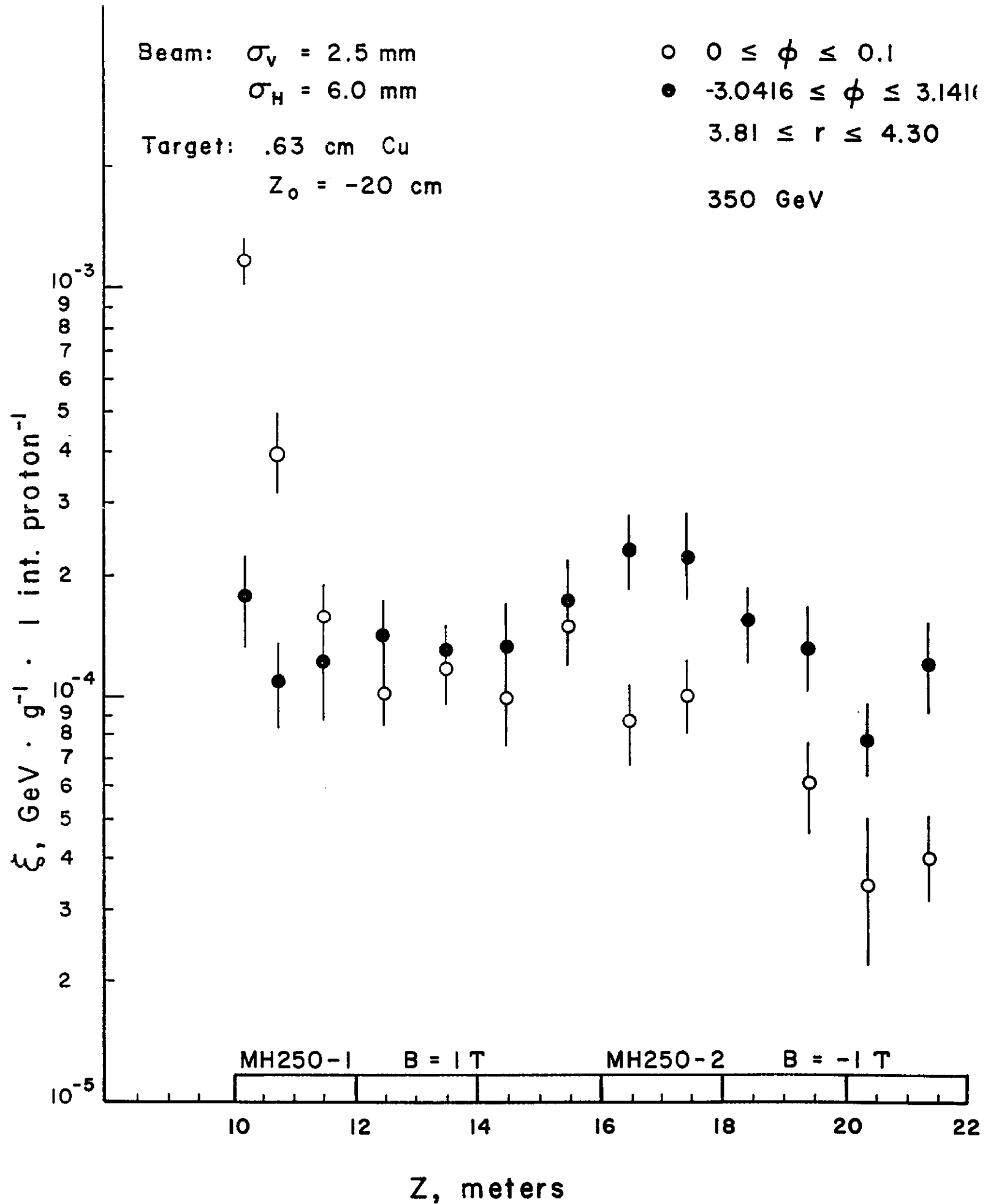


Fig. 6

Beam: $\sigma_V = 2.5$ mm

$\sigma_H = 6.0$ mm

Target: .63 cm Cu

$Z_0 = -20$ cm

○ $0 \leq \phi \leq 0.1$

● $-3.0416 \leq \phi \leq 3.1416$

$3.81 \leq r \leq 4.30$

$15 \leq \delta \leq 50\%$

400 GeV

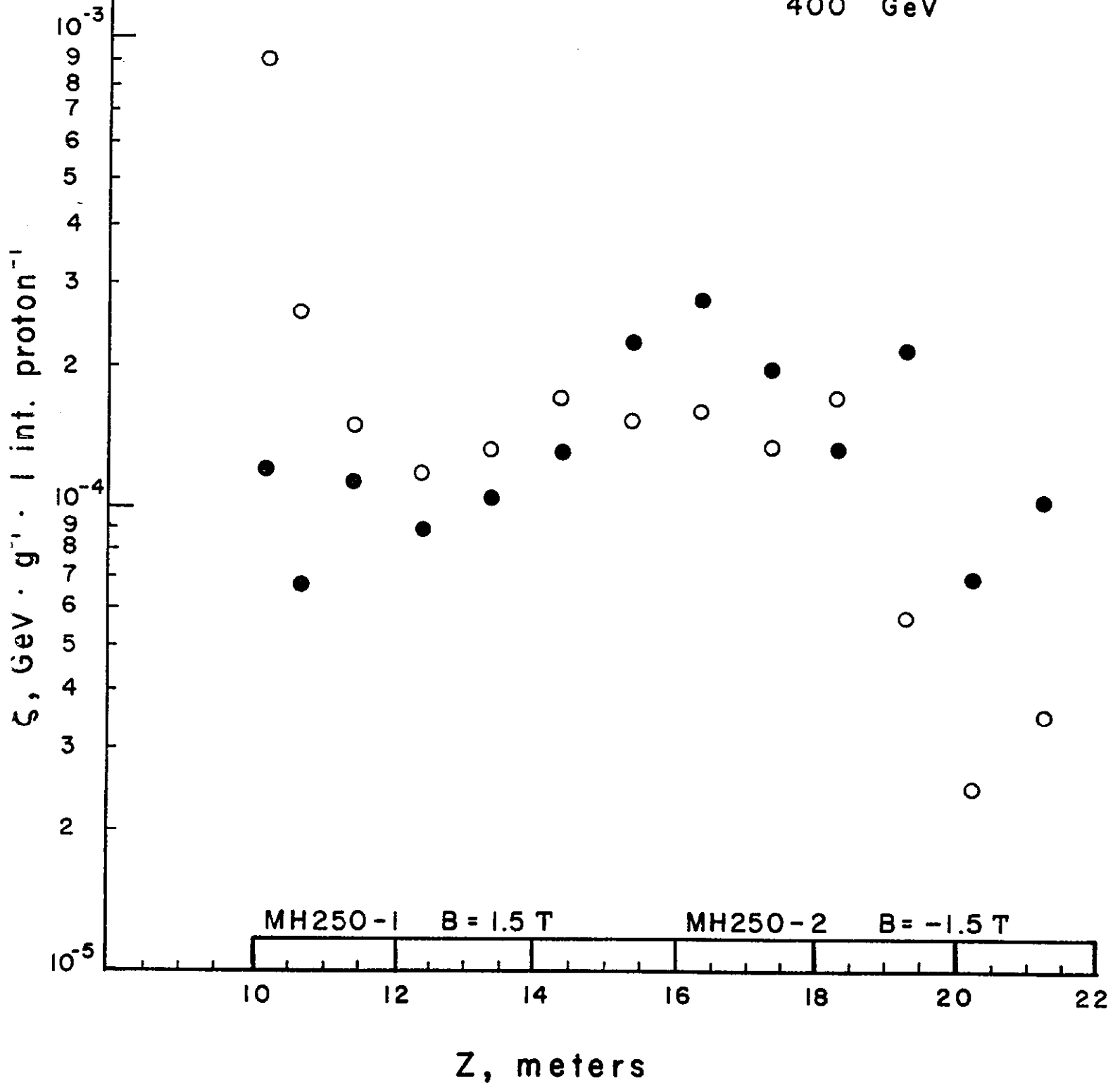


Fig. 7

Beam: $\sigma_v = 2.5$ mm
 $\sigma_H = 6.0$ mm
 Target: .63 cm Cu
 $Z_0 = -20$ cm

○ $0 \leq \phi \leq 0.1$
 ● $-3.0416 \leq \phi \leq 3.1416$
 $3.81 \leq r \leq 4.30$
 $10 \leq \delta \leq 30\%$

400 GeV

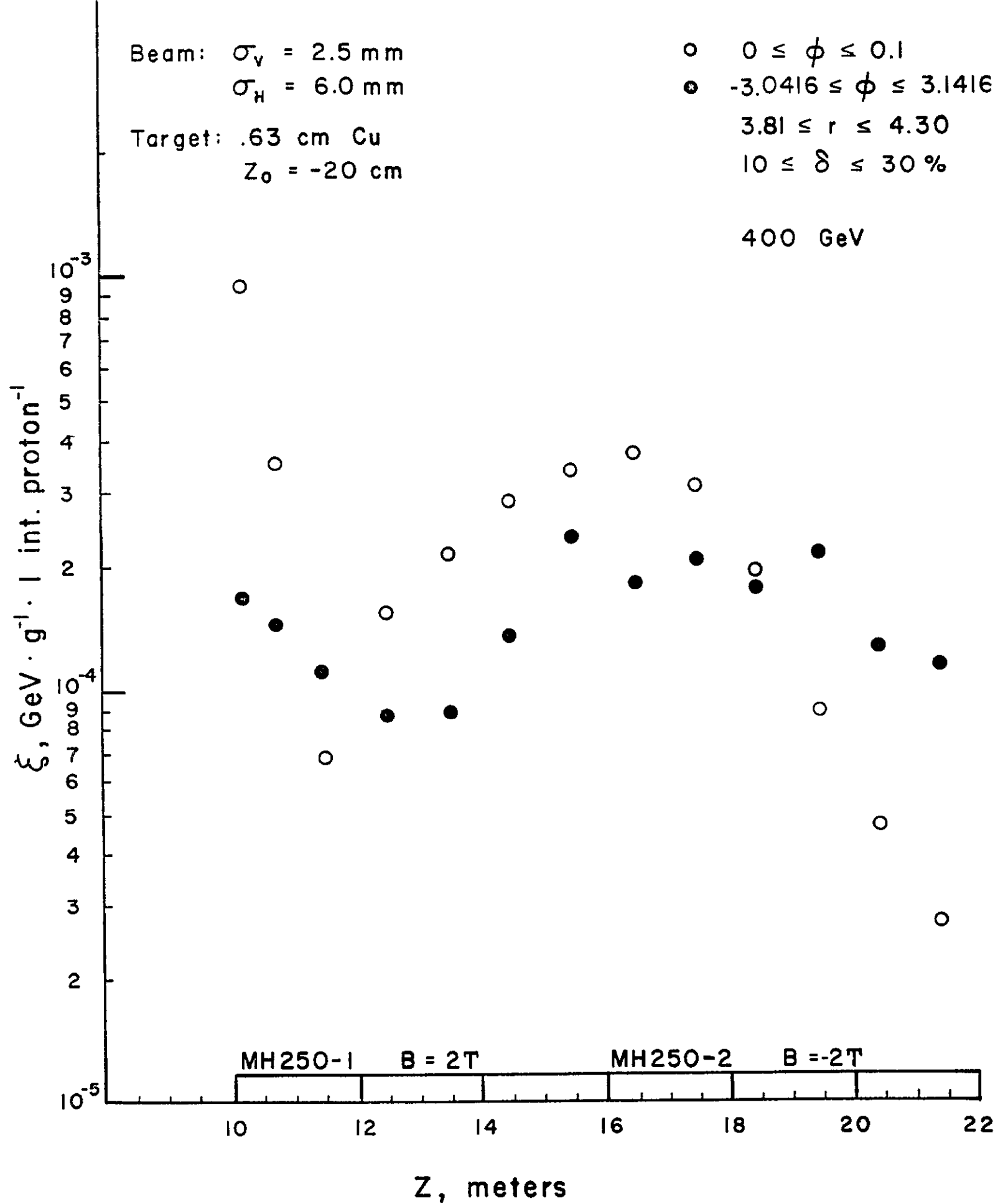


Fig. 8

Beam: $\sigma_v = 2.5$ mm
 $\sigma_H = 6.0$ mm
 Target: .63 cm Cu
 $Z_0 = -20$ cm

$\circ 0 \leq \phi \leq 0.1$
 $\bullet -3.0416 \leq \phi \leq 3.1416$
 $3.81 \leq r \leq 4.30$
 $10 \leq \delta \leq 30\%$
 400 GeV

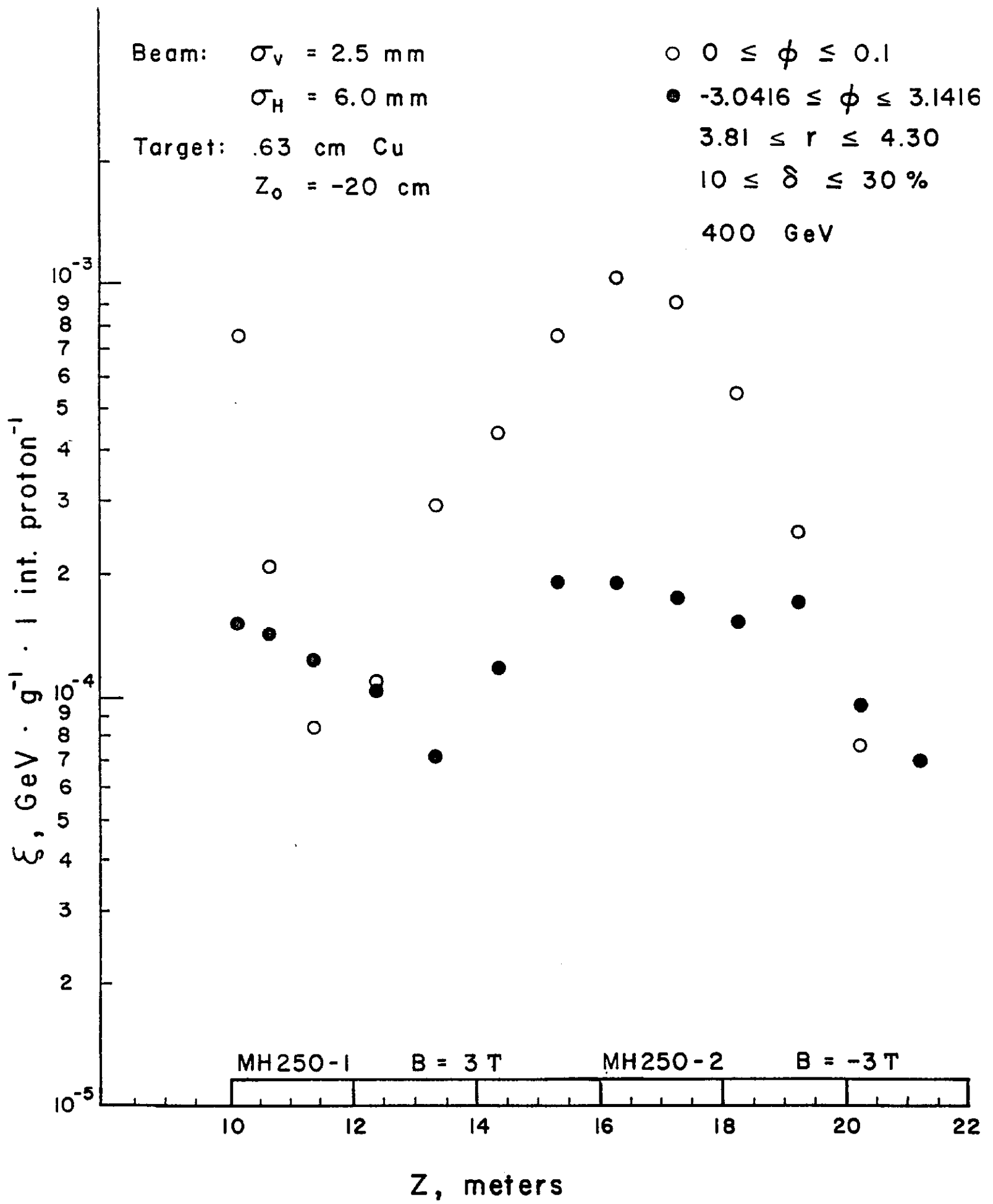


Fig. 9

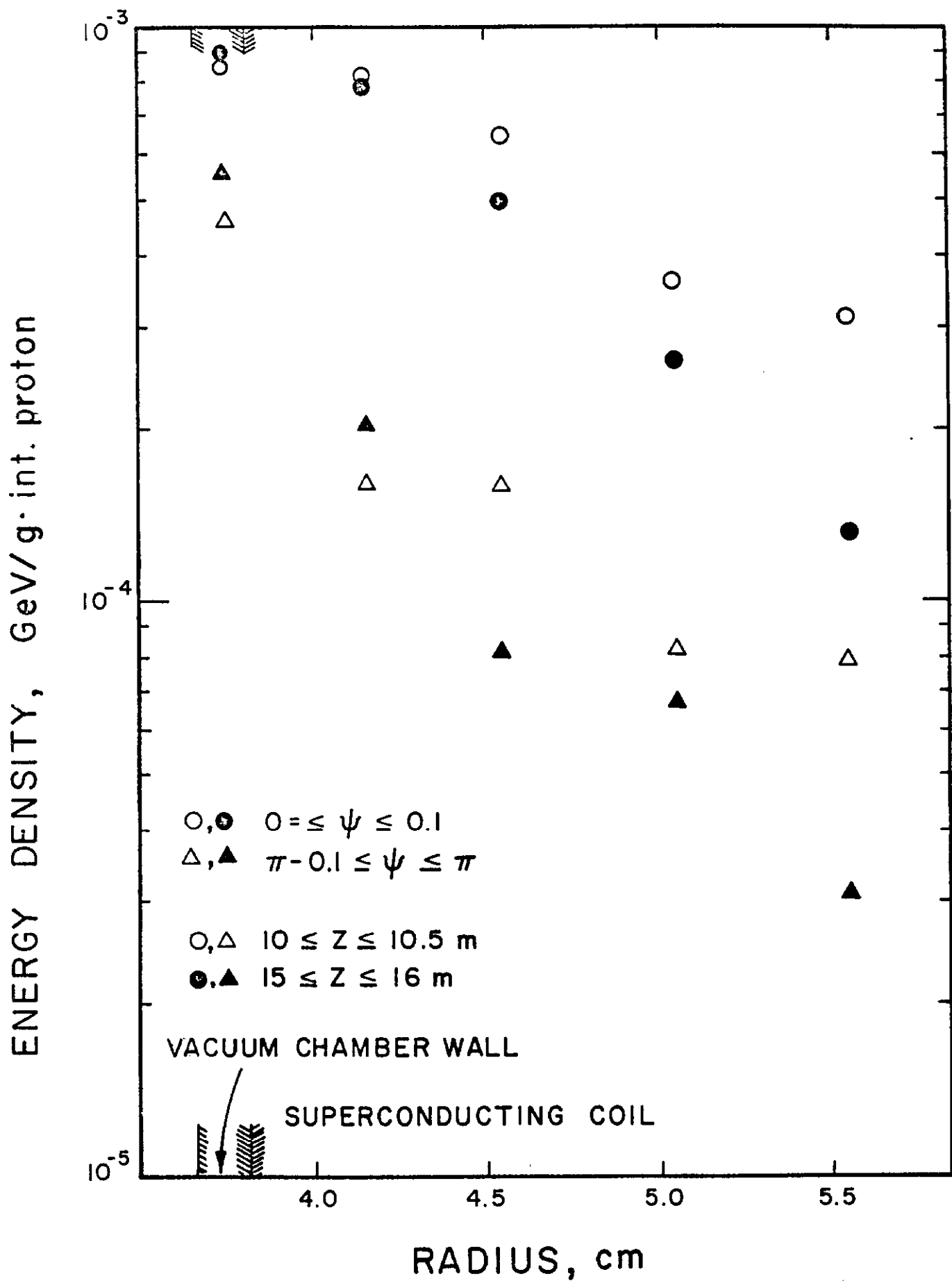


Fig. 10

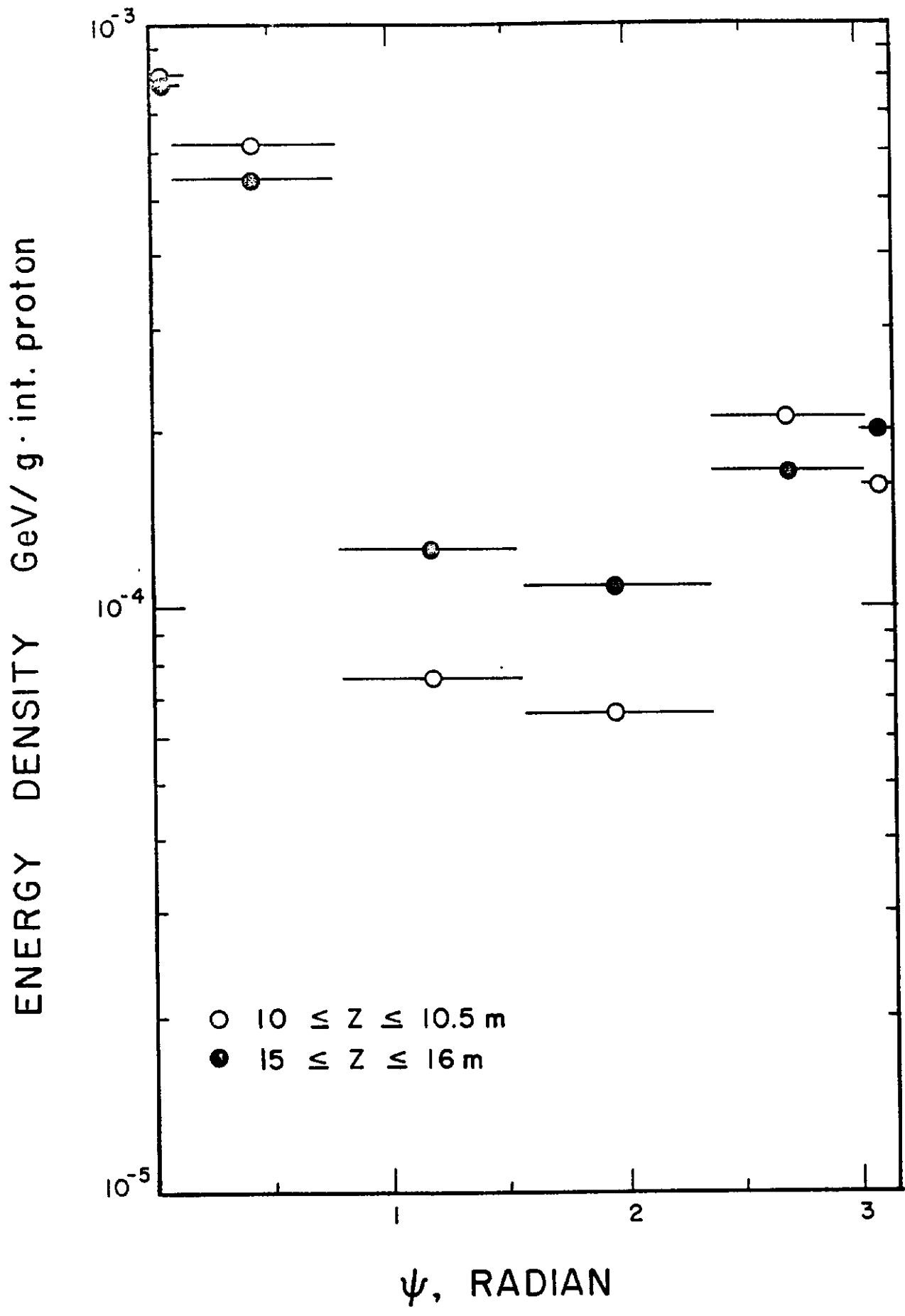


Fig. 11

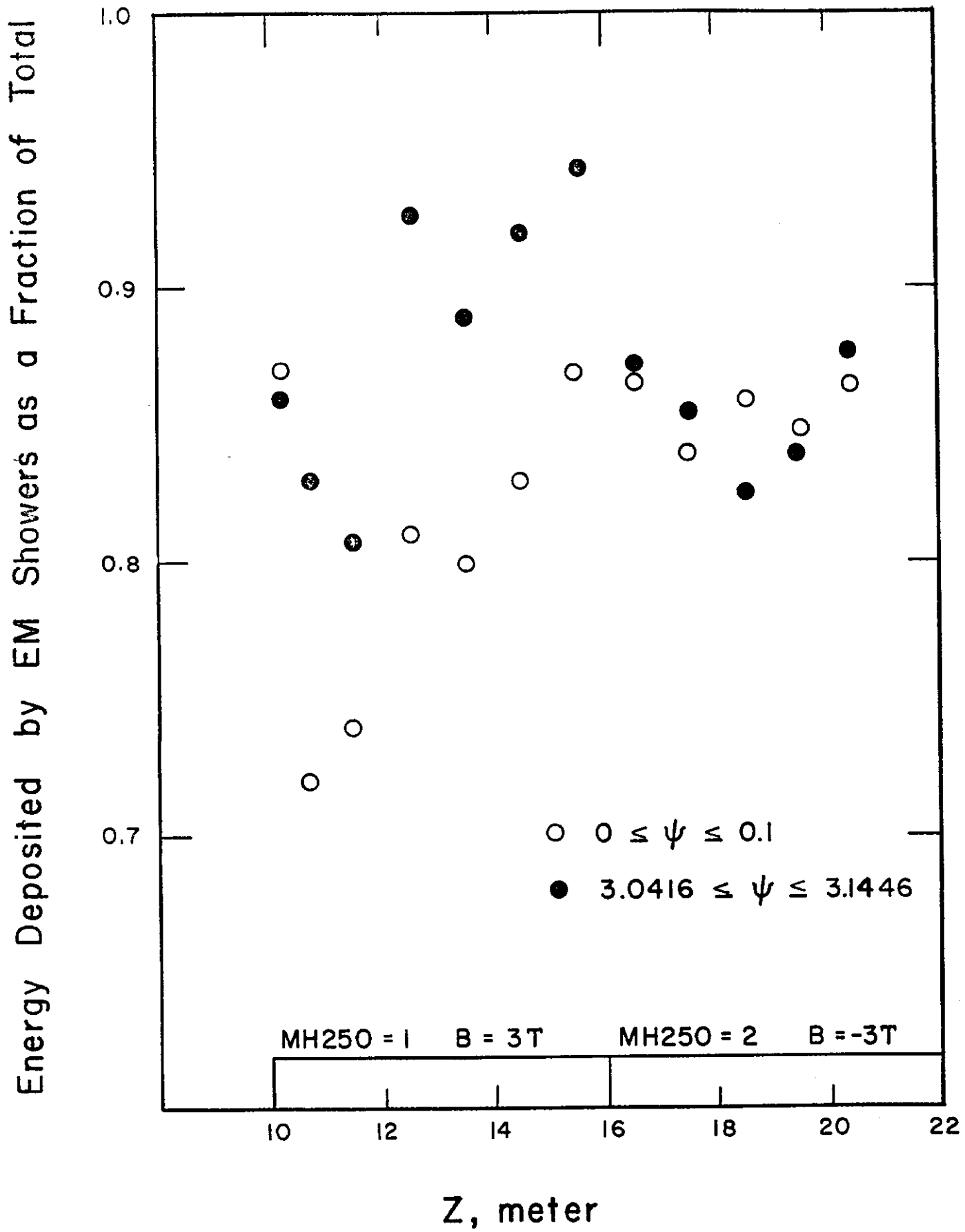


Fig. 12

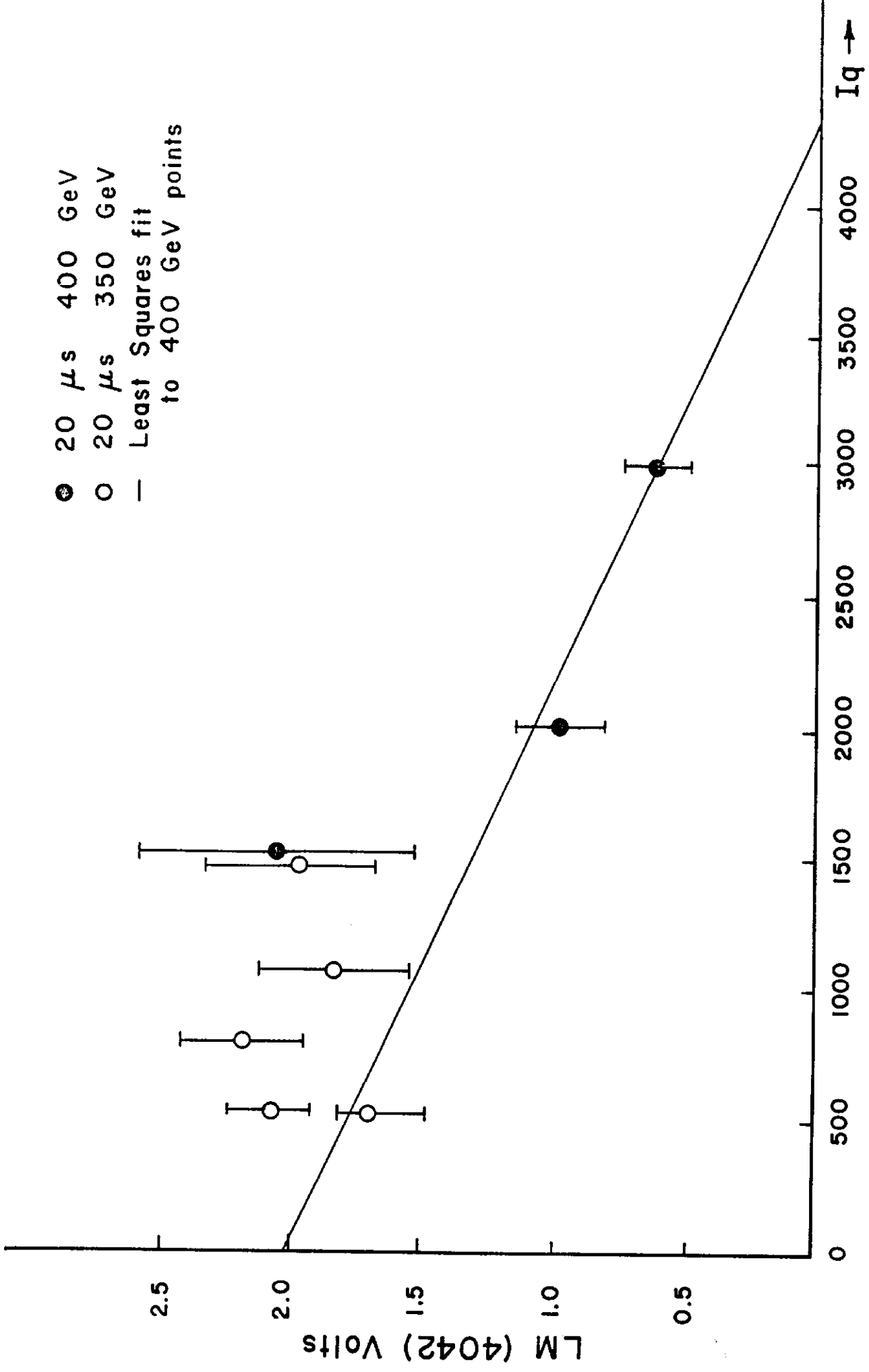


Fig. 13

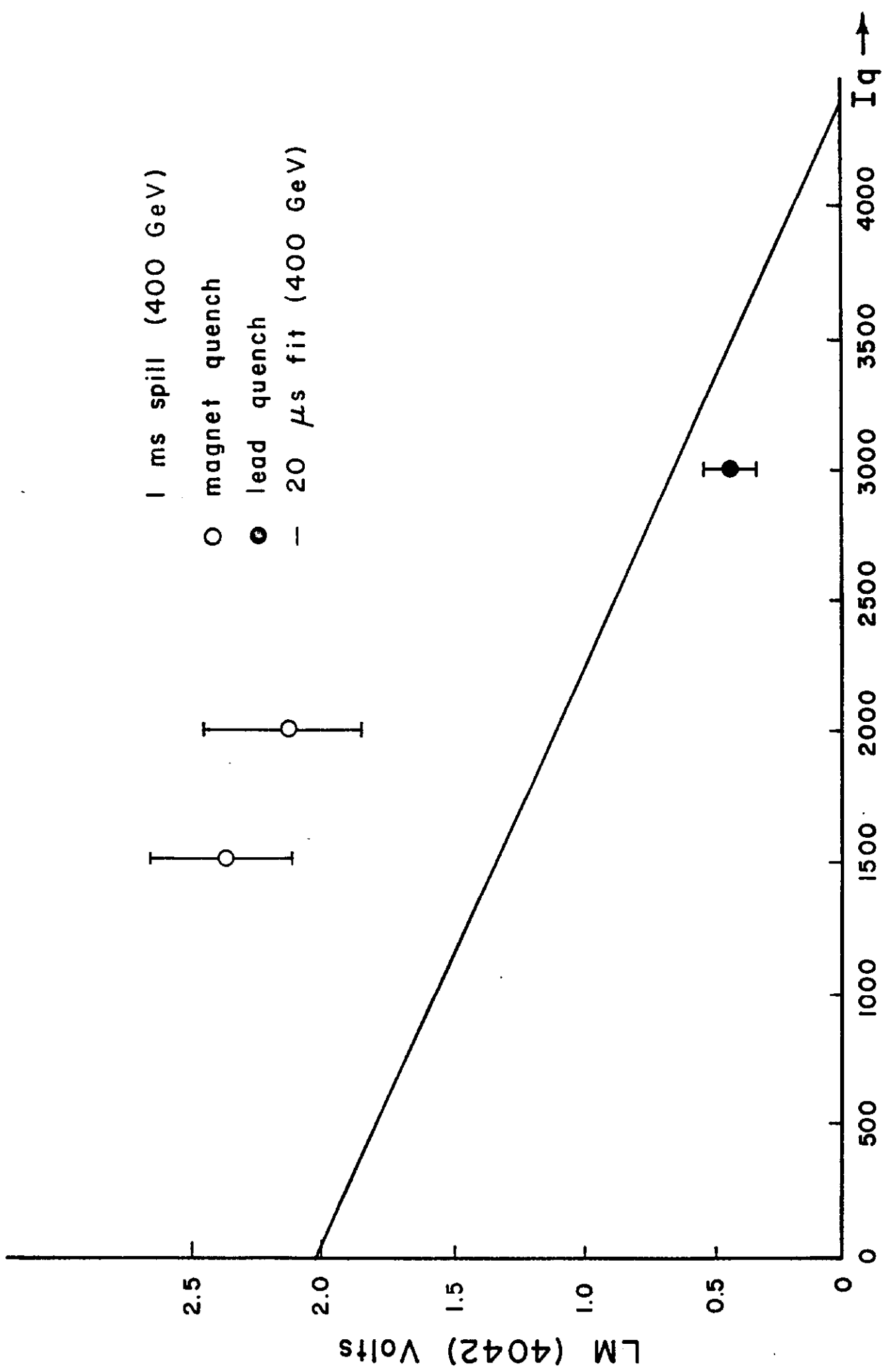


Fig. 14

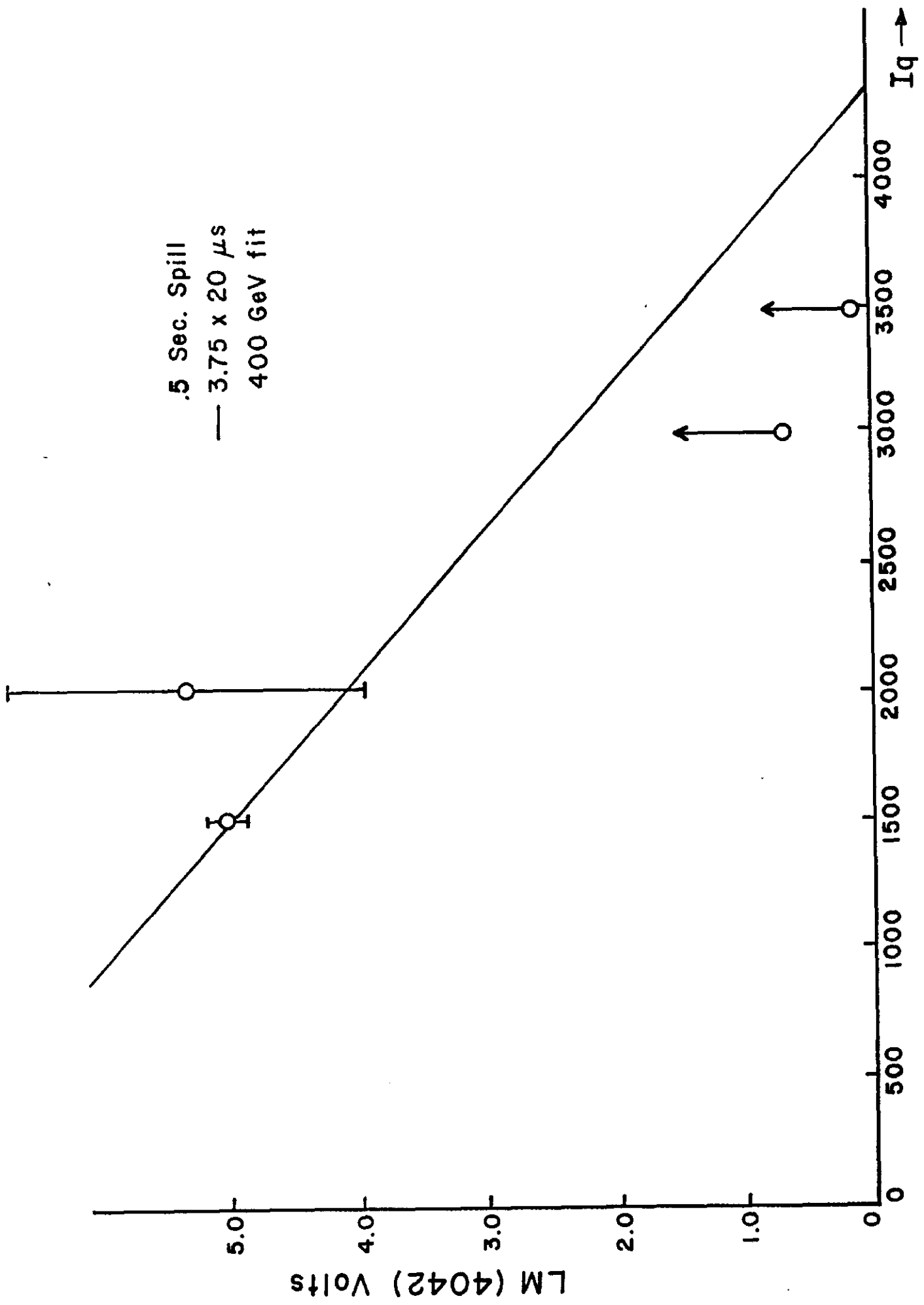


Fig. 15

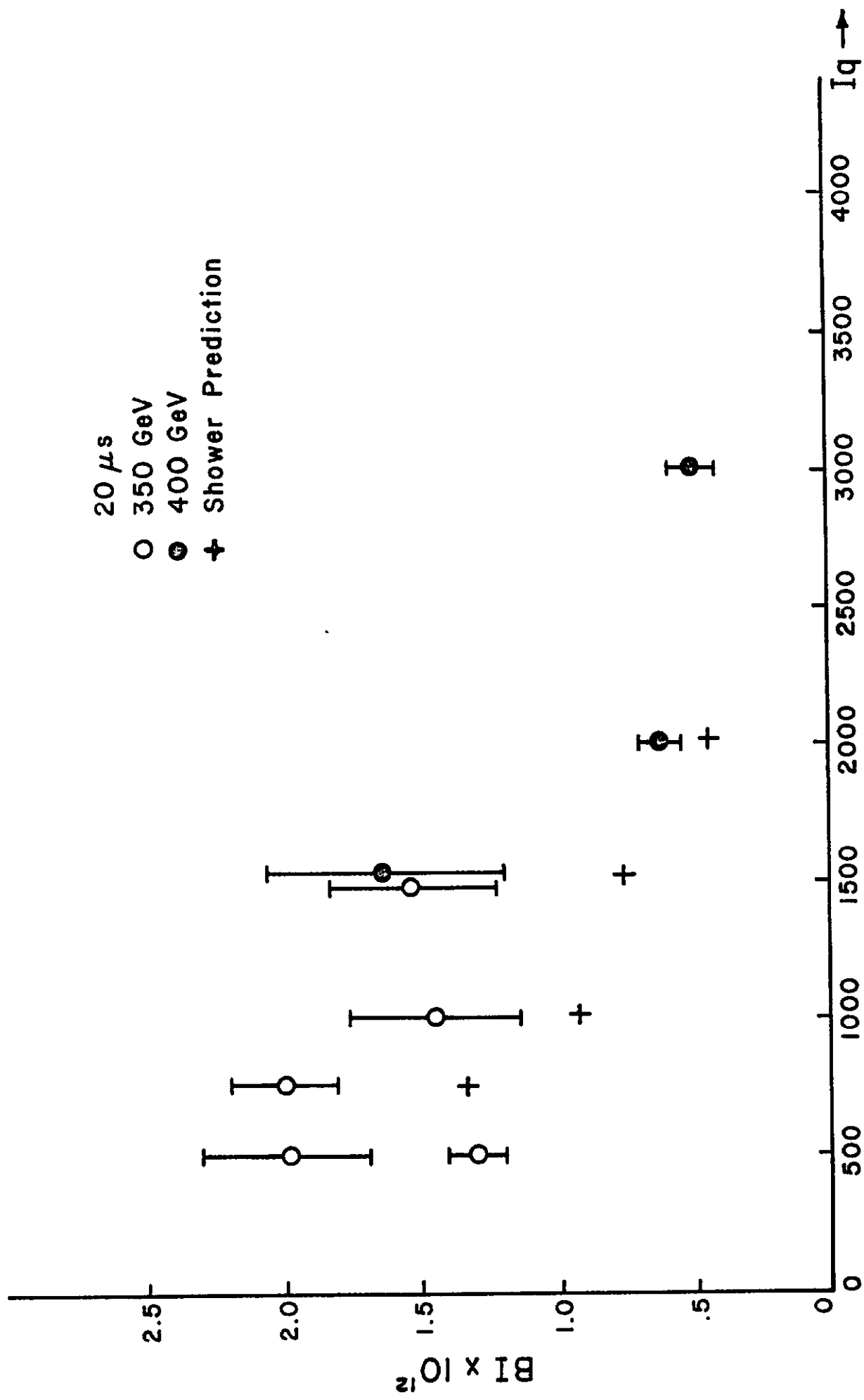


Fig. 16

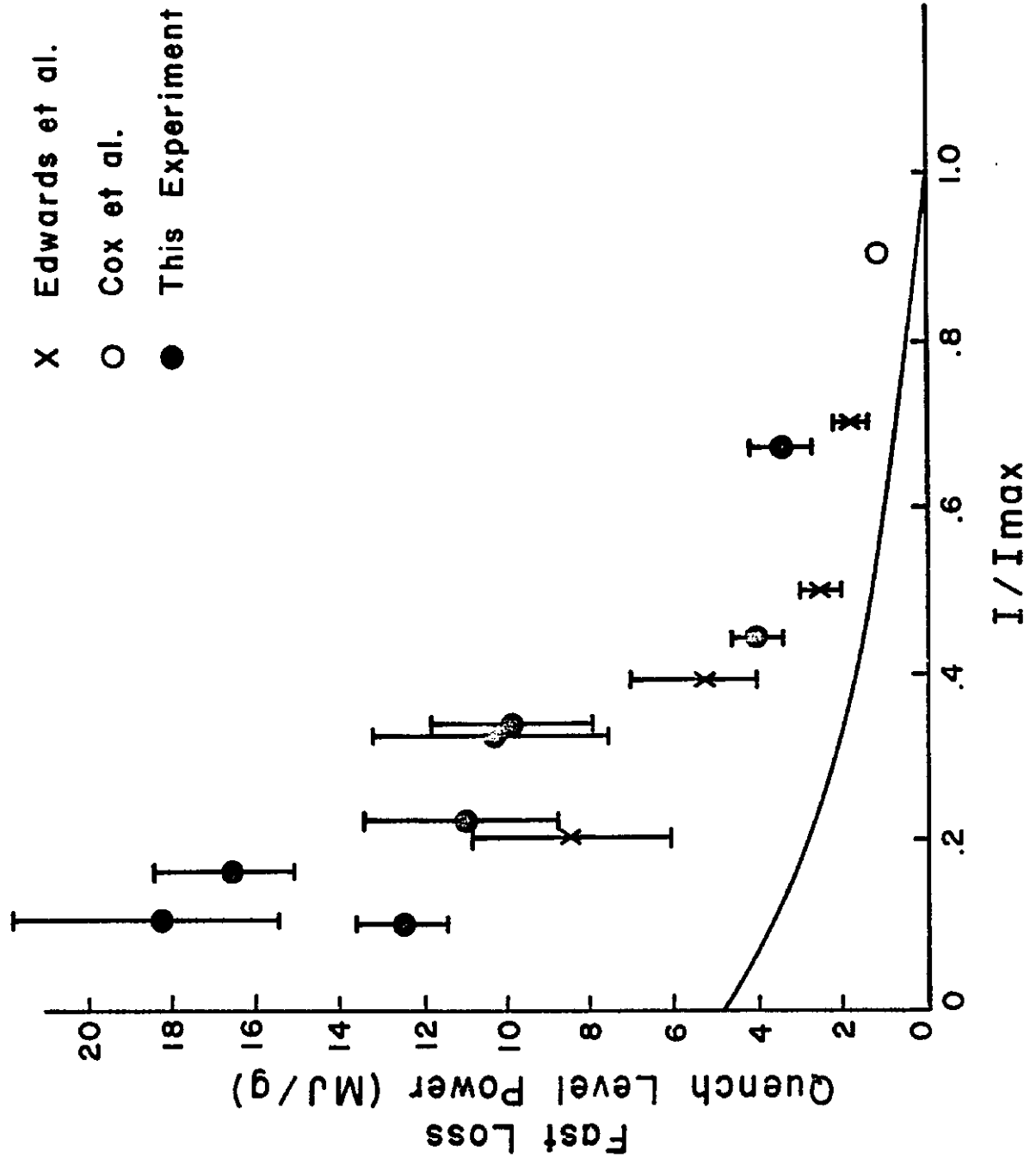


Fig.17